2017

Morphometrics in Developmental Neurobiology: Quantitative Analysis of Growth Cone Motility in Vivo

Anokh Sohal
Touro University California

James Ha
Touro University California

Manuel Zhu
Touro University California

Fayha Lakhani
Touro University California

Lauren Olszewski
Touro University California

See next page for additional authors

Recommended Citation

Sohal, A., Ha, J., Zhu, M., Lakhani, F., Olszewski, L., Mohanakrishnan, R., . . . Elul, T. (2017). Morphometrics in developmental neurobiology: Quantitative analysis of growth cone motility in vivo. In P. M. Pares-Casanova (Ed.), New insights into morphometry studies (pp. 31-45). Rijeka, Croatia: IN TECH.

Chapter 3

Morphometrics in Developmental Neurobiology: Quantitative Analysis of Growth Cone Motility *in Vivo*

Anokh Sohal, James Ha, Manuel Zhu, Fayha Lakhani, Kavitha Thiagaragan, Lauren Olzewski, Raagav Monakrishnan and Tamira Elul

Additional information is available at the end of the chapter

http://dx.doi.org/10.5772/intechopen.69060

Abstract

In order for the nervous system to function properly, neurons in the brain must establish specific connections during embryonic development. Formation of neuronal circuits involves axons extending from cell bodies and navigating through diverse tissues to reach their targets in the brain. Once axons reach their target tissues, they arborize and make synaptic connections. Axon pathfinding is driven by dynamic motility behaviors expressed by terminal growth cones at the tips of the axons. Here, we applied morphometrics to determine quantitative values for six morphological and motility parameters for growth cones of optic axons navigating through the optic tract of a living brain preparation from a *Xenopus laevis* tadpole. Our results demonstrate an increase in length, decrease in width, increase in perimeter, decrease in area, increase in number of filopodia, and a decrease in number of lamellipodia, of the growth cones in the optic tract. Therefore, optic axonal growth cones become less circular and more elongated and protrusive during their navigation through the optic tract. Quantitatively deconstructing parameters of growth cone motility is necessary to determine molecular, cellular, and biophysical mechanisms of axon pathfinding, and to formulate computational analyses of developing neuronal connectivity in the brain.

Keywords: morphometrics, axon, growth cone, optic axons, filopodia, lamellipodia, optic tract, *Xenopus laevis*

1. Introduction

In order for the nervous system to function properly, accurate wiring of the brain must be established during embryonic development. Wiring of the brain depends in large part on axons extending from neuronal cell bodies and subsequently navigating through tissues to reach appropriate targets in the brain. Axon pathfinding is driven by specific and patterned motility behaviors expressed by growth cones at the terminal ends of the axons. Quantitatively deconstructing distinct motility parameters of growth cones will aid studies exploring the molecular and mechanical control of axonal pathfinding, as well as facilitate the development of computational analyses of growth cone motility. Here, we have applied morphometric analyses to determine values, and spatiotemporal patterns in those values, for six parameters of motility from a time-lapse video of two growth cones of optic axons navigating through the optic tract of a living brain preparation from a young *Xenopus laevis* tadpole.

During embryonic development of the visual system, optic neurons extend axons from the eye to the tectal midbrain, where they make synaptic connections essential for visual function. The ability of these optic axons to navigate and propel through the optic tract, and to eventually reach the tectum, is due to the growth cone of the axon. The growth cone is a highly motile structure located at the distal end of the axon that mediates its directional growth and extension by interacting with molecular and mechanical cues in the environment. The growth cone can be divided into three sub-compartments, the peripheral (P), transitional (T), and central (C) domains (**Figure 1**). The P-region of the growth cone contains a meshwork of

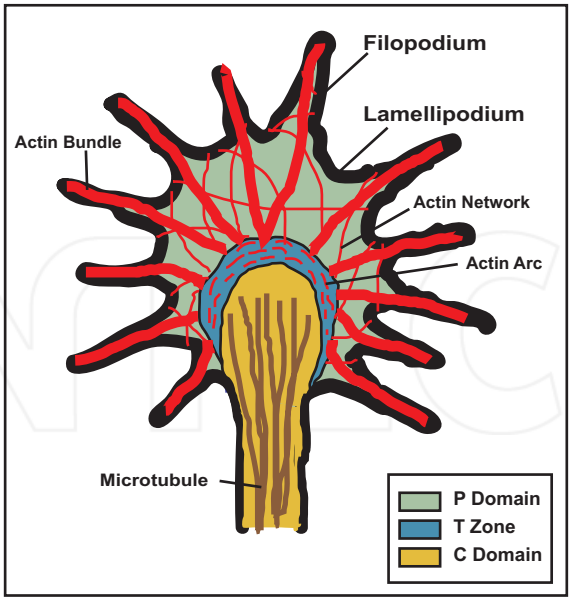

Figure 1. Schematic of growth cone with intracellular domains and protrusions demarcated.

actin filaments and long parallel bundles of actin filaments that underlie two types of protrusions (**Figure 1**). Lamellipodia are short and broad protrusions that are thought to function to generate force for the growth cone advance (**Figure 1**). Filopodia are long and finger-like, and primarily sense the environment and guide the axon (**Figure 1**; [1]). A combination of actin treadmilling and retrograde actin flow allows for continual remodeling of the P-region (and of the lamellipodia and filopodia within this region), required to generate growth cone motility. ATP-actin is assembled into filaments in the distal P-region and then transported rearward to the T-region as polymeric F-actin. In the T-region, F-actin is polymerized and recycled back to ATP-actin and the cycle restarts. Actin is transported retrograde from the P region to the T-region via a myosin motor driven process [2]. The C-region, which is proximal to the P-region, is filled with a dense microtubule array and cellular organelles like mitochondria that support growth cone movement (**Figure 1**; [1]). The microtubule system within the C-region affects cell motility by steering growth cone advance in response to guidance cues from the P-region [3]. The plus end of microtubules exhibits dynamic instability, cycling through periods of growth and shrinkage, allowing them to probe the intracellular space [2]. Similar to actin, microtubules are involved in a transport mechanism involved in maintaining the axon and the growth cone. The majority of microtubules are found in the axon shaft and are stationary. However, in active regions like the growth cone, stable microtubules are tyrosinated to become dynamic [2].

As the growth cone progresses, the P-region senses changes in the extracellular environment, and relays those cues to the C-region. These cues can be either attractive or repulsive [4]. Although the majority of microtubules end in the C-region, single microtubules protrude into the filopodia of the P-region, mediating interaction between the actin and microtubule cytoskeleton (**Figure 1**; [1]). Interactions between microtubules and actin in filopodia are necessary for growth cones to turn. Microtubule and actin interactions also occur in the T zone and C domain of the growth cone, where actin arcs in the T zone exert compressive forces on microtubules in the C domain, facilitating microtubule bundling and aiding in axon navigation (**Figure 1**; [5]). Previous and current studies from our laboratory show that molecules downstream of Cadherin and Wnt signaling ligands such as β-catenin and APC, that regulate the actin and microtubule cytoskeleton, modulate optic axon growth cone morphology and motility in the optic tract as well as targeting and branching in the optic tectum [6, 7]. More generally, it is now clear that the actin and microtubule cytoskeleton of the two growth cone regions are dynamically related, and may influence each other via signaling molecules such as APC [8]. The functional studies of APC *in vitro* from other laboratories also suggest that APC is crucial for growth cone advance and turning [5].

In order to gain a better understanding of the motility, and morphological dynamics of the growth cone, we quantitatively analyzed an *in vivo* time-lapse image sequence of retinotectal axon pathfinding in living brains from *X. laevis* tadpoles. Initial observation of the time-lapse sequence showed that optic axonal growth cones change their morphology and motility depending on where they are in the retinotectal circuit (**Figure 2**). Conceptually, progressing through the optic tract, the growth cone requires greater propulsive properties to get to the tectum but as it reaches the tectum, these propulsive properties decrease as the goal becomes to start making branches and individual synapses with target neurons. We can better understand

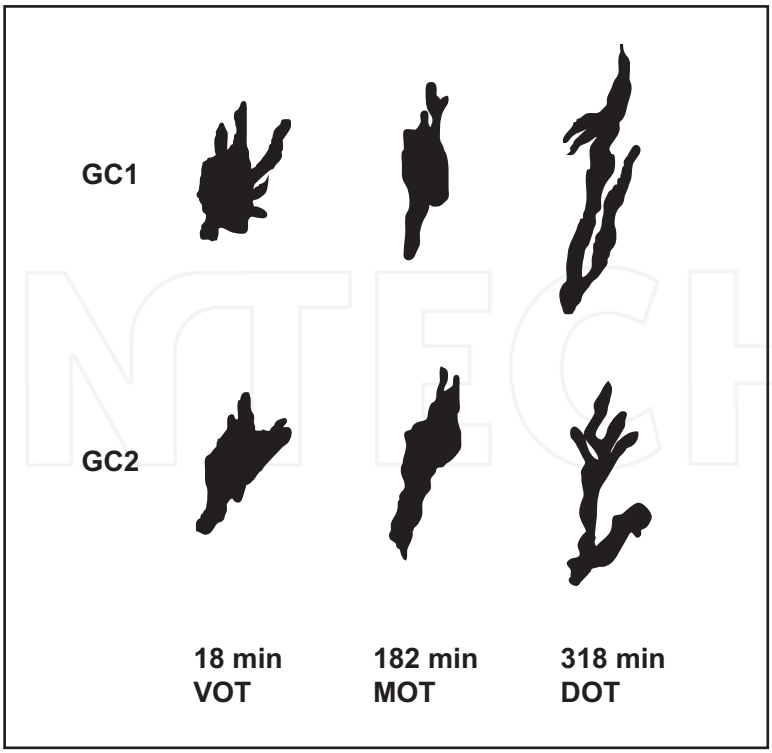

Figure 2. Tracings of still images of two optic axonal growth cones in the optic tract taken from a time-lapse video illustrates how their morphology changes as they navigate through the optic tract. GC1: growth cone 1; GC2: growth cone 2; VOT: ventral optic tract; MOT: mid optic tract; DOT: dorsal optic tract.

how the growth cone behaves and its morphology changes as it progresses through the retinotectal circuit by measuring parameters such as length and width, perimeter and area, and number of filopodial and lamellipodial projections at each time interval [9]. Measurements of length and width, and of perimeter and area, of the growth cone could reflect the details of how the dynamics of actin and microtubule cytoskeleton interactions change as the axon progresses from navigation and propulsion to synapsing. These morphological observations could also help better explain functions of molecular mechanisms such as microtubule tyrosination on the shape of the growth cone. In addition, quantifying the number of filopodial and lamellipodial projections on the growth cones could suggest information on the types of extracellular cues the growth cone is responding to, and their effects on branching of filopodia as the growth cone nears the tectum [9]. Also, observing and quantifying filopodial and lamellipodial morphology could potentially aid researchers to better understand the retrograde actin flow and how it links to the microtubule cytoskeleton through intracellular signaling. Observing and analyzing these different morphological parameters can lead to a better understanding of how intracellular signaling molecules such as β-catenin and APC, or mechanical cues such as tension, affect growth cone motility as well.

2. Methods

An *in vivo* time-lapse video of *X. laevis* optic axons navigating in the optic tract and dorsal tectum was made by Sonia Witte in Christine Holt's laboratory at Cambridge University (http://www.pdn.cam.ac.uk/directory/christine-holt; also see Ref. [10]). The video was a collection of 119 individual frames captured at 3-min time intervals of two GFP-expressing growth cones of optic axons navigating through the optic tract of a living brain preparation taken from a young tadpole at approximately developmental stage 33/34 (**Figure 3**; [11]). The time-lapse video sequence encompassed an approximately 6-h (357 min) time period during which two growth cones (labeled with membrane bound GFP) navigate through the optic tract. Analysis of the two growth cones in each frame was performed using the image analysis software ImageJ (NIH, Bethesda, Maryland, USA). Before beginning the analysis, criteria were

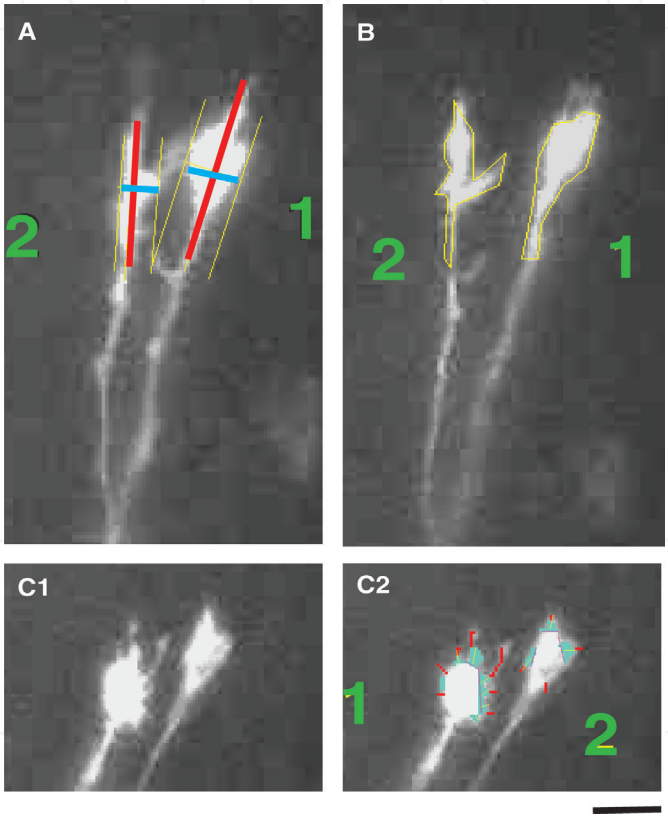

Figure 3. Still images from the time-lapse video sequence of two GFP-labeled optic axons in a living brain preparation from a young *Xenopus laevis* tadpole. (A) Marking for length (thick vertical line) and width (thick horizontal line) measurements of growth cones. (B) Outlines of growth cones for perimeter and area measurements. (C1) Growth cones with protrusions evident. (C2) Filopodia (thin lines) and lamellipodia (thick lines) are marked in the growth cones. Numbers indicate growth cones 1 and 2. Scale Bar—10 μm.

established to standardize the measurements of growth cone parameters (**Figure 3**). A scale bar was set based on a previous publication showing growth cones of optic axons in living brain preparations from *X. laevis* embryos [10].

The length of each growth cone was determined by drawing a line extending along the axonal axis, from the base to the leading edge of the growth cone (thick vertical lines, **Figure 3A**). The base of the growth cone was defined as the first protrusion of the growth cone near the axon shaft (thick lines, **Figure 3A**; [9]). The leading edge of the growth cone was established as the tip of the growth cone, including all protrusions. Width of the growth cone was measured by creating two parallel lines to the length line, at the tips of the distal edges of the growth cone (including its protrusions) (thin vertical lines, **Figure 3A**). The perpendicular distance between these two parallel lines was measured as the maximal width of the growth cone (thick horizontal lines, **Figure 3A**; [9]). This was done for both growth cones for each frame of the time-lapse sequence.

To measure the perimeter of the growth cones, the growth cone boundaries were traced using the polygon drawing tool in ImageJ (yellow outlines, **Figure 3B**). The base of the growth cone was used as the starting point, and the distal edges of the growth cone were traced until reaching the starting point. Similar to the measurement of growth cone length, the base of the growth cone was determined to be where the first protrusion of the growth cone near the axon shaft was located and the growth cone boundary contained all protrusions of the growth cone (**Figure 3B**). Filled area was calculated using the measurement tool in ImageJ.

The number of filopodia and lamellipodia in each image was measured using ImageJ as well (thin lines- filopodia, thick lines - lamellipodia, in **Figure 3C**). Criteria for identifying filopodia and lamellipodia were based on a previous review studying cellular protrusions *in vitro* [12]. This report stated that lamellipodia can vary from 1 to 5 μm in width. Therefore, any protrusions extending from the growth cone body between 1 and 5 μm in width were considered lamellipodium, and any protrusions less than 1 μm in width were considered filopodia. The number of filopodial and lamellipodial protrusions was recorded for both growth cones in each frame.

To avoid researcher-dependent bias in morphometric measurements, five different researchers performed the measurements for length, width, perimeter, and area on the two growth cones at each time point, using the protocols described above. Their values were averaged to obtain final measurements for these size parameters for the growth cones at each time point. All measurements (length, width, area, perimeter, and number of filopodia and lamellipodia) were initially plotted against time in a scatter plot. However, to better display the changes in the data, and to depict the changes in the growth cones as they progressed from ventral, to mid, to finally, the dorsal optic tract, we subdivided the time-lapse video into three time bins. The time-lapse video was composed of 119 frames at 3-min intervals, spanning a total time of 357 min. Therefore, first time bin encompassed 3–117 min (39 images), the second 120–237 min (39 images), and the third 240–357 min (39 images). Averages were calculated for the morphometric measurements for each of the three time groups for both growth cones, and then averages of those averages were determined over the two growth cones. These average growth cone parameters were plotted on bar graphs to determine if there were any differences between their values during the three time bins (**Figures 4–6**).

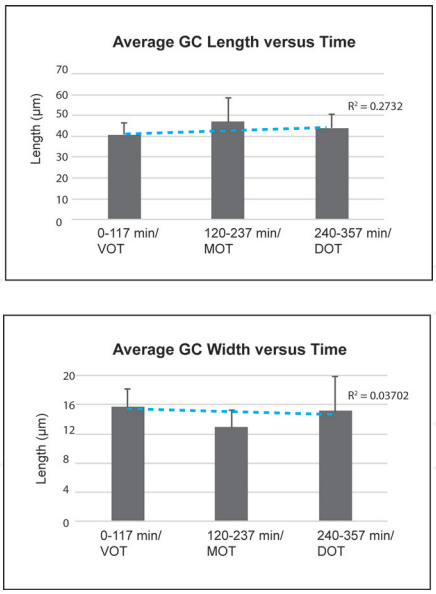

Figure 4. Plots of average growth cone length and width versus time. VOT: ventral optic tract; MOT: mid optic tract; DOT: dorsal optic tract.

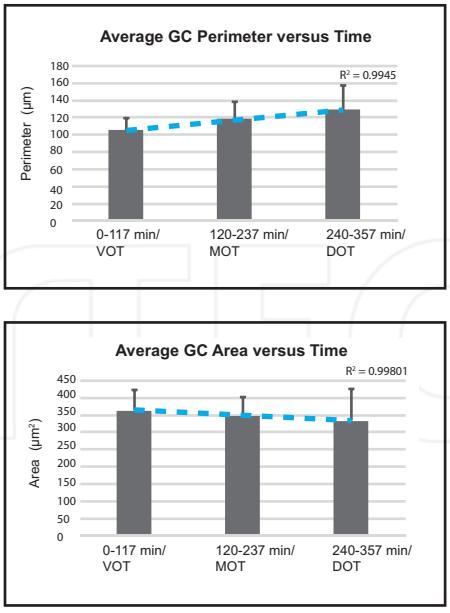

Figure 5. Plots of average growth cone perimeter and area versus time. VOT: ventral optic tract; MOT: mid optic tract; DOT: dorsal optic tract.

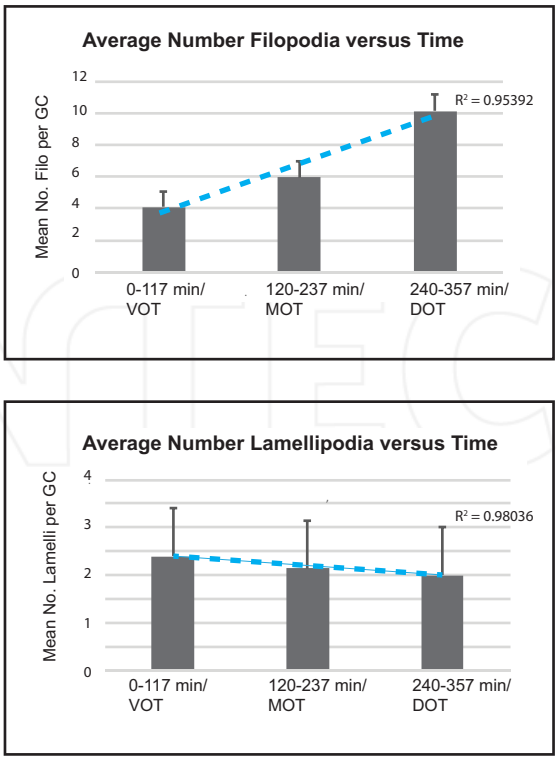

Figure 6. Plots of mean number of filopodia and lamellipodia per growth cone versus time. VOT: ventral optic tract; MOT: mid optic tract; DOT: dorsal optic tract.

3. Results

3.1. Quantitative analysis shows morphological changes in growth cones *in vivo*

3.1.1. Growth cone length increases, while width decreases over time

The lengths and widths of the growth cones were measured using specific criteria described in Section 2. Measurements were taken for both growth cones in each of the 119 frames of the time-lapse video. The time-lapse video was broken up into three equal time bins, and the average length and width for the growth cones were calculated for each of the time bins and plotted on bar graphs (**Figure 4**). Trend lines were added to the graphs. The results revealed that as the growth cones progressed through the optic tract, on average, their length increased, and their width decreased (**Figure 4**). However, the length of the growth cones increased a smaller amount than their width decreased during their navigation through the optic tract (**Figure 4**).

The mean length for growth cone one was initially 45.9 μm (*SD* = 2.52 μm, *n* = 39 images), in the ventral optic tract/time bin one. The mean length for growth cone one increased to

47.9 μm (*SD* = 0.78 μm, *n* = 39 images), in the third time bin, corresponding to the dorsal optic tract. The mean length for growth cone two was initially 35.7 μm (*SD* = 8.8 μm, *n* = 39 images), in the ventral optic tract/time bin one. The mean length for growth cone two increased to 40 μm (*SD* = 12.04 μm, *n* = 39 images), in the third time bin, or the dorsal optic tract. On average, the two growth cones increased their lengths by 8% (*SD* = 5.5%, *n* = two growth cones) as they progressed from the ventral to the dorsal optic tract. This corresponds to an average rate of increase of length of 1.4%/h (*SD* = 0.92%/h, *n* = two growth cones) for growth cones of optic axons navigating in the optic tract.

The mean width for growth cone one was initially 16.1 μm (*SD* = 1.81 μm, *n* = 39 images), in time bin one, or the ventral optic tract. The mean width for growth cone one changed to 13.9 μm (*SD* = 3.61 μm, *n* = 39 images), in the third time bin, corresponding to the dorsal optic tract. The mean width for growth cone two was initially 15.3 μm (*SD* = 3.12 μm, *n* = 39 images), in time bin one, or the ventral region of the optic tract. The mean width for growth cone two changed to 16.3 μm (*SD* = 5.79 μm, *n* = 39 images), in the dorsal optic tract. For the two growth cones, we calculated an average decrease of width of approximately 4% (*SD* = 14.3%, *n* = two growth cones) as they navigated through the optic tract of the living brain preparation. This corresponded to an average rate of decrease in growth cone width of 0.6%/h (*SD* = 2.38%/h, *n* = two growth cones) during optic axon navigation from the ventral to the dorsal optic tract.

3.1.2. Growth cone perimeter increases, while area decreases over time

The perimeter and area of the growth cones were measured using the techniques described in Section 2. Measurements were taken for both growth cones in each of the 119 frames. Again, the time-lapse video was decomposed into three equal time bins and average growth cone perimeter and area were calculated for each of the time bins and plotted as bar graphs with trend lines (**Figure 4**). The results revealed that, on average, the growth cone perimeter increased, and the area decreased as the optic axons progressed through the optic tract (**Figure 5**). In addition, the growth cone perimeter increased more than the growth cone area decreased as the optic axons navigated through the optic tract in a living brain preparation (**Figure 5**).

The mean perimeter of growth cone one for time bin one was approximately 112 μm (*SD* = 13.5 μm, *n* = 39 frames), whereas the mean perimeter for growth cone one for the third time bin, corresponding to the dorsal optic tract, increased to 134 μm (*SD* = 30.7 μm, *n* = 39 images). The mean perimeter of growth cone two for time bin one was 98 μm (*SD* = 14.3 μm, *n* = 39 images), whereas the mean perimeter for growth cone two for the third time bin, corresponding to the dorsal optic tract, was 124 μm (*SD* = 26.3 μm, *n* = 39 images). This corresponds to an average increase of 23% (*SD* = 4.9%, *n* = two growth cones) for the perimeter of the growth cones as they navigated through the optic tract. We also calculated an average rate of increase in growth cone perimeter of 3.8%/h (*SD* = 0.8%/h, *n* = two growth cones) during their navigation through the optic tract.

The mean area of growth cone one for time bin one was 392 μm^2 (*SD* = 48.9 μm^2, *n* = 39 images), whereas the mean area for the third time bin, corresponding to the dorsal optic tract was decreased to 346 μm^2 (*SD* = 112.3 μm^2, *n* = 39 images). The mean area of growth cone two for time bin one

was 333 μm^2 (*SD* = 71.1 μm^2, *n* = 39 images), whereas the mean area for growth cone two for the third time bin, corresponding to the dorsal optic tract was 321 μm^2 (*SD* = 71.3 μm^2, *n* = 39 images). On average, the two growth cones decreased their area by 8.6% (*SD* = 6.65%, *n* = two growth cones) during their navigation through the optic tract. This corresponds to a rate of decrease of area of 1.4%/h (*SD* = 1/1%/h, *n* = two growth cones) for optic axonal growth cones in the optic tract.

3.1.3. Filopodial protrusions increase, and lamellipodial protrusions decrease over time

To further decompose growth cone motility in the optic tract, the number of filopodial and lamellipodial protrusions in the growth cones was measured using criteria described in Section 2. The number of protrusions was calculated for both growth cones in each of the 119 frames of the time-lapse sequence. The average number of filopodia and lamellipodia for the growth cones for each of the time bins were calculated and plotted as bar graphs with trend lines (**Figure 6**). The results revealed that the mean number of filopodial protrusions increased, and the mean number of lamellipodial protrusions decreased, as the growth cones navigated through the optic tract toward the optic tectum (**Figure 6**). However, the mean number of filopodia per growth cone increased much more than the mean number of lamellipodia decreased during the time the optic axons extended through the optic tract (**Figure 6**).

The mean number of filopodia in growth cone one during time bin one (117 min) or the ventral optic tract was 4.4 (*SD* = 1.69, *n* = 39 images), whereas the mean number of filopodia for this growth cone for the third time bin, corresponding to the dorsal optic tract, was 10.3 (*SD* = 1.49, *n* = 39 frames). The mean number of filopodia displayed by growth cone two during time bin one was 3.8 (*SD* = 1.48, *n* = 39 images), whereas the mean number of filopodia for this growth cone in the third time bin, corresponding to the dorsal optic tract, increased to 10 (*SD* = 2.1, *n* = 39 images). On average, the two growth cones increased their average number of filopodia by 148% (*SD* = 16.6%, *n* = two growth cones), or at a rate of 25%/h (*SD* = 2.8%/h, *n* = two growth cones).

The mean number of lamellipodia of growth cone one for time bin one was 2.4 (*SD* = 0.97, *n* = 39 images), whereas the mean number of lamellipodia for the third time bin, corresponding to the dorsal optic tract, was 2.1 (*SD* = 0.68, *n* = 119 images). The mean number of lamellipodia of growth cone two for time bin one was 2.4 (*SD* = 0.75, *n* = 39 images), whereas the mean number of lamellipodia for the third time bin, corresponding to the dorsal optic tract decreased to 1.9 (*SD* = 0.63, *n* = 39 images). On average, the two growth cones decreased their average number of lamellipodia by 17% (*SD* = 5.3%, *n* = two growth cones), which corresponds to a mean rate of decrease of lamellipodia of 2.8%/h (*SD* = 0.87%/h, *n* = two growth cones).

4. Discussion

4.1. Changes in optic axonal growth cone morphologies in the optic tract

This quantitative analysis of growth cone motility of the *in vivo* time-lapse video demonstrates six morphological changes in growth cones of optic axons navigating in the optic tract of *X. laevis* brains. There was an increase of length, decrease of width, increase in perimeter, decrease in area, increase in number of filopodia, and a decrease in number of lamellipodia of the growth

cones (**Figures 4–6**). These results show that as the growth cones progress through the optic tract, they become less circular, and more elongated and protrusive (**Figure 2**). These findings could help us gain a better understanding of the intracellular changes that may be influencing the morphology of the growth cones. From *in vitro* and *in vivo* studies, we know that growth cones comprise three domains: the C-domain composed of microtubules, the T-domain containing actin arcs, and the P-domain composed of actin as well (**Figure 1**). The P-domain has also filopodial protrusions, composed of actin bundles, and lamellipodial protrusions, composed of a meshwork of actin (**Figure 1**; [1–3]). The change in the morphology of the growth cone as it progresses through the optic tract could be due to the intracellular changes in these filaments. As the growth cone loses its circularity and becomes a more protrusive structure, microtubules could be consolidating in the axon shaft, and actin could be remodeling to influence the growth cone morphology once it reaches the dorsal optic tract. The changes in morphology of the growth cone could also be due to the different extracellular cues, such as Netrins, Wnts, Cadherins and CAMS, the growth cone encounters as it progresses through the optic tract [13]. One possibility is that there could be more and/or different extracellular cues in the dorsal tectum, causing the growth cone to project more filopodia. Since filopodia sense extracellular cues and are composed of actin bundles, this could mean that actin bundles take a prominent role, whereas microtubules in the C-domain of the growth cone begin to play a less important role in the structure of the growth cone. The predominance of bundled actin could also be attributed to decreased retrograde actin flow or to changes in motor driven transport proteins like Myosin II [14]. How actin and microtubules communicate these extracellular cues to intracellular changes could in turn be due to signaling molecules like APC that bind both actin and microtubules. Microtubules may become less predominant as the axons reach the end of the tract because of increased levels of APC within the growth cone [15–17]. APC could also influence retrograde actin flow in the growth cone. These intracellular molecular mechanisms underlying growth cone form and motility could be examined with further research. It is clear through analysis of the time-lapse video that specific morphological changes in the growth cone do occur in the optic tract. Our quantitative analysis can help us refine our understanding of the complicated intracellular mechanisms present within the growth cone.

4.2. Previous quantitative analysis of growth cones of optic axons *in situ*

Previous study quantified morphologies of growth cone of optic axons in the optic tract of brains from *X. laevis* tadpoles [18]. In this earlier study, growth cones of optic neurons injected with Lucifer yellow dye were examined in the optic tract in transverse sections of fixed brains. From the images of these growth cones, the author measured size parameters (area, length, and width), as well as number of processes in different regions of the optic tract. However, there were several differences between these previous measurements of growth cone parameters in fixed brains and the measurements we present here based on a living brain preparation. First, the previous study defined the base of the growth cone as the region of the axon where there was an abrupt thickening, or as the point halfway between the thickest region of the growth cone and the axon [18]. In contrast, we defined the base of the growth cone as the point where the first protrusion of the growth cone appeared on the axon [9]. In addition, in contrast to our measurement of width of the growth cone at its maximum point, the previous study measured growth cone width at 4–6 different points along the growth cone and

averaged these measurements to obtain a final width [18]. Finally, and most significantly, our growth cone size measurements included the protrusions of the growth cone, whereas these previous growth cone dimensional parameters did not include filopodial or lamellipodial protrusions [18]. These differences in experimental approach (living versus fixed brains) and morphometric criteria (definition of base of growth cone, of width of growth cones, and inclusion or lack thereof of filopodia in growth cone size measurements) between the earlier study and our report clarify why our measured values for width, length, and area of growth cones of optic axons are significantly greater (~2× greater for length, width, and area) than those presented in the previous study. The previous study also applied different criteria for classifying filopodia and lamellipodia in optic axonal growth cones than we did in this study. The author considered filopodia to be protrusions (between 0.2 and 0.5 μm in width) that projected 2 μm or more from the growth cone surface, whereas lamellipodia were processes shorter than 2 μm [18]. In contrast, based on a different study, we considered any protrusion extending from the growth cone body between 1 and 5 μm in width as lamellipodia, and any protrusions less than 1 μm in width as filopodia [12]. However, despite these differences in classification of filopodia and lamellipodia, we counted similar numbers of protrusions in optic axonal growth cones in the ventral and mid-optic tract as in the earlier study.

4.3. Limitations and future directions for measurements of growth cones *in vivo*

In this quantitative analysis of growth cone morphology, researchers measured dimensions and protrusions of growth cones of optic axons manually outlining and delimiting boundaries of growth cones themselves (based on set criteria). One concern with having human researchers perform morphometric analyses is the potential variability in their delimitation of growth cone boundaries, and accordingly, the lack of reproducibility in their measurements. To circumvent this issue, we had five different researchers who make the same morphometric measurements on the two growth cones in each frame of the time-lapse sequence. We then averaged the values obtained by the different researchers to calculate our final values for size measurements of growth cone morphologies. Another approach to ensure reproducibility in quantitative analysis of growth cone morphology would be to have an automated computer program performing the measurements. However, before applying an automated approach, several issues would need to be resolved. First, the growth cones would need to be resolved with computer vision in a three-dimensional brain (**Figure 3**). Most automated algorithms work well on growth cones imaged *in vitro* (in two-dimensional cultures) but have difficulty establishing realistic boundaries for growth cones imaged in intact, three-dimensional tissues. Second, one would need to algorithmically define the base of the growth cone using a specific criterion, such as the point of the first protrusion on the axon near the growth cone. Currently, any automated computer program that is able to perform this type of analysis on extending axons and growth cones *in vivo* is not known.

In addition, in this study, we measured morphometric parameters for a relatively small number of growth cone of optic axons based on a time-lapse video captured of two fluorescently-labeled growth cones navigating in the optic tract of a single living brain preparation. Therefore, it is possible that our measurements are not representative of growth cones of optic axons in living brains generally. Instead, our growth cone measurements may be biased by the experimental conditions of this brain preparation. For example, the pressure exerted by the cover slip on the

living brain preparation can alter the morphology of the growth cones as they navigate through the optic tract. To expand and generalize these morphometric measurements, we would need to make measurements on additional GFP expressing growth cones in different living brain preparations. An appropriate sample number would be 10–15 growth cones in five different living brain preparations. This would allow us to determine whether our morphometric measurements are generally representative of growth cones of optic axons from *X. laevis* tadpoles.

Limitations notwithstanding, the detailed measurements that we made of growth cone parameters advance our understanding of the dynamics of optic axon pathfinding in the optic tract of *X. laevis* brains *in vivo*. Our study establishes a template for the types of morphometric measurements that could be made from additional time-lapse video sequences of optic axons navigating in the optic tract of living brains. In the future, the motility parameters we measured for optic axonal growth cones of *Xenopus* brains could be compared to similar parameters obtained for growth cones of other types of neurons in different tissues. This would allow researchers to determine in a precise, quantitative manner how growth cone motility varies in different cell types and/or species. Moreover, this detailed quantitative analysis of growth cone motility of wild type optic axons will be fundamental for future studies examining how mechanical and molecular cues regulate the growth cone motility of optic axons *in vivo*. Finally, researchers aiming to develop computational visualizations of growth cone motility could use the quantitative parameters we measured for optic axonal growth cones to develop more accurate *in silico* representations of developing axonal connectivity in neuronal projections [19].

Acknowledgements

We thank Sonia Witte for making the time-lapse video of GFP-labeled optic axons in a living brain preparation from a *X. laevis* tadpole (http://www.pdn.cam.ac.uk/directory/christine-holt; also see Ref. [10]). We are grateful to Christine Holt for allowing us to use this time-lapse video as the basis for this morphometric study of optic axonal growth cones in the optic tract *in vivo*.

Funding for this project was provided by the Masters in Medical Health Sciences program in the College of Osteopathic Medicine at Touro University California. Publication made possible in part by support from the Berkeley Research Impact Initative (BRII) sponsored by the UC Berkeley Library.

Author details

Anokh Sohal[1], James Ha[1], Manuel Zhu[1], Fayha Lakhani[1], Kavitha Thiagaragan[2], Lauren Olzewski[1], Raagav Monakrishnan[1] and Tamira Elul[1]*

*Address all correspondence to: tamira.elul@tu.edu

1 Touro University California, Vallejo, California, United States of America

2 University of California, Berkeley, Berkeley, California, United States of America

References

[1] Vitriol EA, Zheng JQ. Growth cone travel in space and time: The cellular ensemble of cytoskeleton, adhesion and membrane. Neuron. 2012;**73**(6):1068-1081. DOI: 10.1016/j.neuron.2012.03.005

[2] Dent EW, Gertler FB. Cytoskeletal dynamics and transport in growth cone motility and axon guidance. Neuron. 2003;**40**(2):209-227

[3] Lowery LA, Van Vactor D. The trip of the tip: Understanding the growth cone machinery. Nature Reviews Molecular Cell Biology. 2009;**10**(5):332-343. DOI: 10.1038/nrm2679

[4] Mueller BK. Growth cone guidance: First steps towards a deeper understanding. Annual Review of Neuroscience. 1999;**22**:351-388. DOI: 10.1146/annurev.neuro.22.1.351

[5] Geraldo S, Gordon-Weeks PR. Cytoskeletal dynamics in growth cone steering. Journal of Cell Science. 2009;**122**(20):3595-3604. DOI: 10.1242/jcs.042309.

[6] Wiley A, Edalat K, Chiang P, Mora M, Mirro K, Lee M, Murh H, Elul T. GSK-3beta and alpha-catenin binding regions of beta-catenin exert opposing effects on the terminal ventral optic axonal projection. Developmental Dynamics. 2008;**237**(5):1434-1441. DOI: 10.1002/dvdy.21549

[7] Elul TM, Kimes NE, Kohwi M, Reichardt LF. N- and C-terminal domains of beta-catenin, respectively, are required to initiate and shape axon arbors of retinal ganglion cells *in vivo*. Journal of Neuroscience. 2003;**23**(16):6567-6575.

[8] Ettienne-Manneville S. Actin and microtubules in cell motility: Which one is in control? Traffic. 2004;**7**:470-477. DOI: 10.1111/j.1600-0854.2004.00196.x.

[9] Bray D, Chapman K. Analysis of micro spike movements on the neuronal growth cone. Journal of Neuroscience. 1985;**12**:3204-3213

[10] Harris WA, Holt CE, Bohoeffer F. Retinal axons with and without their somata, growing to and arborizing in the tectum of Xenopus embryos: A timelapse video study of single fibres *in vivo*. Development. 1987;**101**(1): 123-133

[11] Nieuwkoop PD, Faber J. Normal Table of *Xenopus laevis*. Amsterdam: Daudin; 1956

[12] Small JV, Stradal T, Vignal E, Rottner K. The lamellipodium: Where motility begins. Trends Cell Biology. 2002;**12**(3):112-120

[13] Hynes RO, Lander AD. Contact and adhesive specificities in the associations, migrations, and targeting of cells and axons. Cell. 1992;**68**(2):303-322

[14] Vallee RB, Seale GE, Tsai JW. Emerging roles for myosin II and cytoplasmic dynein in migrating neurons and growth cones. Trends Cell Biology. 2009;**7**:347-355. DOI: 10.1016/j.tcb.2009.03.009

[15] Purro SA, Ciani L, Hoyos-Flight M, Stamatakou E, Siomou E, Salinas PC. Wnt regulates axon behavior through changes in microtubule growth directionality: A new role for adenomatous polyposis coli. Journal of Neuroscience. 2008;**28**(34):8644-8654. DOI: 10.1523/JNEUROSCI.2320-08.2008

[16] Votin V, Nelson WJ, BArth AI. Neurite outgrowth involves adenomatous polyposis coli protein and beta-catenin. Journal of Cell Science. 2005;**118**(24):5699-5708. DOI: 10.1242/jcs.02679

[17] Zhou FQ, Zhou J, Dedhar S, Wu YH, Snider WD. NGF-induced axon growth is mediated by localized inactivation of GSK-3beta and functions of the microtubule plus end binding protein APC. Neuron. 2004;**42**(6):897-912. DOI: 10.1016/j.neuron.2004.05.011

[18] Holt CE. A single-cell analysis of early retinal ganglion cell differentiation in Xenopus: From soma to axon tip. Journal of Neuroscience. 1989;**9**:3123-3145

[19] Buettner HM. Computer simulation of nerve growth cone filopodial dynamics for visualization and analysis. Cell Motility and the Cytoskeleton. 1995;**32**(3):187-204. DOI: 10.1002/cm.970320304

INTECH